Journal of Materials Chemistry A

Accepted Manuscript

ROYAL SOCIETY OF CHEMISTRY

www.rsc.org/materialsA

Journal of Materials Chemistry A RSCPublishing

ARTICLE

Mixed matrix membranes with molecular-interaction-driven tunable free volumes for efficient bio-fuel recovery

Cite this: DOI: 10.1039/xoxxoooooox

Received ooth XXXX 2014,
Accepted ooth XXXX 2014

DOI: 10.1039/xoxxoooooox

www.rsc.org/

Gongping Liu,[a] Wei-Song Hung,[b] Jie Shen,[a] Qianqian Li,[a] Yun-Hsuan Huang,[b] Wanqin Jin,[*, a] Kueir-Rarn Lee,[*,b] and Juin-Yih Lai[b]

Mixed matrix membranes (MMMs), consisting of inorganic fillers dispersed in a polymer matrix, are regarded as one of the most promising futuristic membranes. This work reported on utilizing molecular interactions to finely control the conformation and topology of polymer chains to fabricate high-performance polyhedral oligomeric silsesquioxanes (POSS) /polydimethylsiloxane (PDMS) MMMs. The influence of POSS incorporation on the polymer structure was systematically studied by molecular dynamics simulation combined with DSC, XRD and IR measurement. The surface and interfacial morphologies of the MMMs were observed through SEM, TEM and AFM characterizations. In particular, positron annihilation spectroscopy was employed to analyze the evolution of free volumes in the MMMs. Results indicated that facilely incorporating POSS into PDMS by molecular interactions could manipulate favorable interfacial morphology and tunable free volumes in MMMs. In the PDMS MMMs, the small free volumes were reduced and the large free volumes increased; these changes were beneficial for the preferential permeation of large-sized molecules through the polymeric membrane. As applied to the bio-butanol recovery from aqueous solutions, the prepared POSS/PDMS MMMs exhibited a simultaneous increase in permeability and selectivity, breaking the permeability-selectivity trade-off limitation, meanwhile transcending the upper bound of the state-of-the-art organophilic pervaporation membranes. Therefore, our work demonstrates that the proposed approach based on rationally creating molecular interactions can be expected to have broad applicability in fabricating high-quality MMMs for molecular separations.

Introduction

The transport of small molecules through nano-pores in rigid materials or free volumes in soft matters continues to receive tremendous attention in the fields of batteries[1], packing materials[2], catalysis[3] and organisms[4], etc. This nanoscopic phenomenon also drives the development of membrane technologies based on molecular-scale separations, such as gas separation[5, 6], pervaporation[7, 8], and ions separation[9], because of the inherent advantages of energy-saving and cost-effectiveness. Recently, owing to the emerging scarcity of oil resources and the demand for environmental protection, bio-butanol (a typical biofuel) produced from biomass fermentation is important in the development of renewable energies[10]. Nowadays, the low productivity, resulting from the end-product inhibition in the fermentation process, is one of the largest obstacles to the implementation of bio-butanol. The integration of the membrane separation technology with the fermentation process for in-situ butanol removal is considered as a promising approach to improve the bio-butanol productivity[11]. Various researches were reported about the PV recovering n-butanol from ABE model solution or fermentation broth using silicone rubber-based membranes[12-18], poly(ether block amide) (PEBA)-based membranes[19, 20], polyvinylidene fluoride (PVDF) membranes[21], polytetrafluoroethylene (PTFE) membranes[22], as well as MFI zeolite membranes[23]. One of the great demands is membranes with high butanol permeability and selectivity. However, there is a general trade-off between permeability and selectivity for state-of-the-art membranes.

Attempts to overcome the performance limitation are generally based on designing and controlling of the materials chemistry or nanostructure to create more preferential adsorption and diffusion of the target permeating molecules. Currently, incorporating nano-fillers into polymers to fabricate mixed matrix membranes (MMMs) has been proven to be an efficient approach to improve membrane permeability and selectivity[16, 17, 20, 24-27]. Besides of the commonly used zeolites[28, 29], carbon molecular sieves (CMS)[24] and metal-organic

frameworks (MOFs)[16, 17, 20, 27], polyhedral oligomeric silsesquioxane (POSS) has been explored as a nanoparticle filler to fabricate MMMs in recent years[28, 30-32]. POSS is a kind of molecular silica with a cage-like nanostructure that possesses an inner inorganic silicon and oxygen core $(SiO_{1.5})_n$ and external organic substituents[33]. The diverse functional groups and good compatibility with polymers make POSS a promising candidate for pervaporation[28-32], gas separation[8, 30, 34] as well as osmosis processes[35, 36]. Unlike common nanoparticles, POSS is very small (ca. 2 nm) and flexible, which can be functionalized with various groups attached to the apex silicon atoms. Chung's group has carried out lots of interesting work on POSS-derived MMMs[8, 28-30, 34-36]. They demonstrated that POSS provided a high possibility of uniform dispersion in diverse polymer matrices even at the molecular level[8, 28].

Until now, how to effectively avoid inadequate particle dispersion and defective filler-polymer interface are regarded as the key points for achieving high-quality MMMs[37]. Rational methods are critically needed to construct a desirable filler/polymer interface that provides sufficient adhesion between the filler and the polymer and maintains adequate mobility of the polymer chains. By precisely selecting the filler size and polymer structure, Merkel et al.[38] proposed poly(4-methyl-2-pentyne)/fumed silica nano-composite membranes through filler-induced disruption of the polymer chain packing to enhance both gas permeability and selectivity. Research group of Koros[29] reported a deposition of inorganic nanostructures on zeolite crystals for MMMs fabrication. The adsorption and entanglement of polymer chains in the nano-whiskers on zeolite provided enhanced zeolite/polymer adhesion and yielded membranes with significantly improved separation performance. Jiang and co-workers[36] took the synergy of hydrogen bond, metal-organic coordination and π-complexation interactions between dopamine and polymer to reinforce polymer chain rigidity and facilitate the molecular transport in membranes. In addition, it has been reported that filler-polymer interactions play a critical role in determining the compatibility and dispersion of fillers in polymers, as well as the final structural, thermal, and mechanical properties of the nano-composites[39].

This work reported a facile strategy of creating molecular interactions between inorganic molecules and polymer chains to fabricate high-performance MMMs. Our idea aims to finely control the conformation and topology of polymer chains through appropriate intra-molecular and inter-molecular interactions resulting from immobilization and movement of backbone and side chains induced by the incorporated inorganic phase. We demonstrated our finding here with the example of polydimethylsiloxane (PDMS) membrane, a benchmark for organophilic pervaporation (e.g., bio-fuel recovery from dilute aqueous solution, VOCs removal), has relatively low separation performance that are still insufficient for practical applications[40]. POSS was selected to be the inorganic filler for PDMS MMMs, because it can act as a robust inorganic molecule that provides good interfacial adhesions and favorable molecular interactions with PDMS polymer. The resulted tunable PDMS chain structures would enable fast-selective diffusion channels in MMMs for molecular transport. Thus, the separation performance of PDMS MMMs can be expected to fulfil breaking the trade-off limitation between permeability and selectivity. Molecular dynamic simulation and experimental characterizations, such as transmission electron microscopy, atomic force microscopy, and positron annihilation spectroscopy, were carried out to systematically study the membrane microstructures. Separation performance of the as-prepared POSS/PDMS MMMs was evaluated through the bio-butanol recovery from its aqueous solution by pervaporation.

Experimental

Materials

Methyl-POSS ($C_8H_{24}O_{12}Si_8$, OctaMethyl POSS®, MS0830) nanoparticles (particle size: 200-300 nm) were supplied by Hybrid Plastics Inc., USA. PDMS (*α,ω*-dihydroxypolydimethylsiloxane, average molecular weight: 6000) was purchased from Sigma Aldrich. Tetraethylorthosilicate (TEOS), *n*-heptane, dibutyltin dilaurate and *n*-butanol were obtained as analytical regents from Sinopharm Chemical Reagent Co., Ltd, China. Deionized water was used in all experiments. Tubular ceramic substrates were supplied by the Membrane Science & Technology Research Center (MST), Nanjing Tech University. They are asymmetric ZrO_2/Al_2O_3 membranes, with an average pore size of 0.2 μm. Their length, outer diameter, and inner diameter were 62 mm, 12 mm, and 8 mm, respectively.

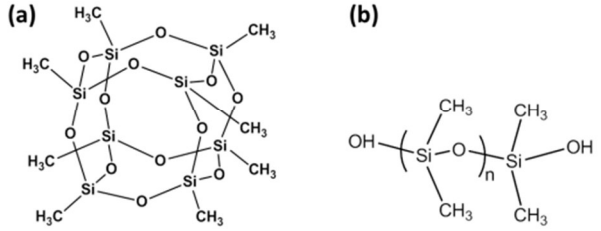

Fig. 1 Molecular structure of (a) OctaMethyl-POSS and (b) ω-dihydroxyl-PDMS used in this work

Molecular dynamics simulation

Molecular models were constructed using the Materials Studio software from Accelrys Incorporation. The model construction and calculation parameters are described as follows. In the Amorphous Cell, the PDMS monomer was selected to construct the PDMS membrane model. The number of repeat units, chain numbers, and initial density of PDMS were set to 25, 4, and 0.9 g/cm^3, respectively[15, 41, 42]. First, the energy minimization process with 3000 iterations was performed to optimize the geometric structure of the membrane model in Forcite. Then, 150-ps NPT (fixed atom number, system pressure, and temperature) with a time step of 1 fs was performed for the MD simulation. Nose algorithm[43] (controlling the thermodynamic temperature and generate the correct statistical ensemble such that the probability of the occurrence of a certain configuration obeys the laws of statistical mechanics) was used to maintain the system temperature at 313 K, and the Q ratio was set as 0.001. Berendsen algorithm[44] (changing the pressure by altering the coordinates of the particles and the size of the unit cell in periodic boundary conditions) was used to maintain the system pressure at 0.001 GPa, and the decay constant was set as 0.5 ps. After the MD simulation of the PDMS model, a certain number of POSS molecules were introduced into the PDMS cell for the construction of POSS/PDMS MMMs models with various POSS content, as shown in Figure 2. Then, the above-mentioned same energy minimization process and NPT calculation were adopted to perform the MD simulation of POSS/PDMS MMM systems. The Condensed-phase Optimized Molecular Potential for Atomistic Simulation Studies

(COMPASS) force field was used to carry out all the model calculations[45].

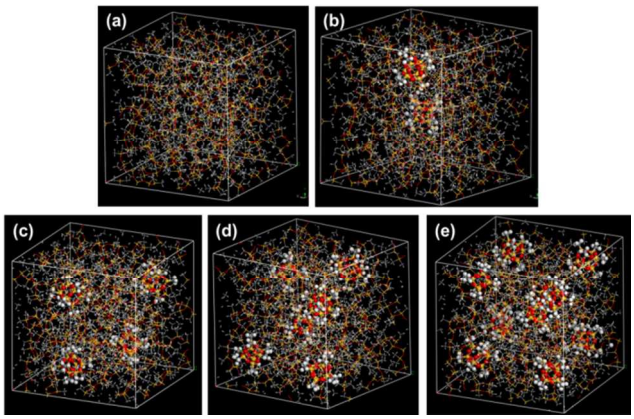

Fig. 2 POSS/PDMS MMMs cells in MD simulation: POSS content: (a) 0 wt%, (b) 10 wt%, (c) 20 wt%, (d) 30 wt%, (e) 40 wt%

Radial distribution function (RDF) was used to analyze the microstructures of PDMS and POSS/PDMS MMMs. This function counts the number of two-atom species within specific distances and is defined as follows:

$$g_{\alpha,\beta}(r) = \frac{V_0}{N_\beta}\frac{N_\beta(r)}{4\pi r^2 \Delta r} \quad (1)$$

where V_o is the cell volume, N_β is the total number of β atoms, and $N_\beta(r)$ is the number of β atoms found within a spherical shell with radius r to $r+\Delta r$, which corresponds to α atoms.

Mean-squared displacement (MSD) was employed to analyze the molecular mobility of membrane, which can be obtained by the Einstein relationship as follows:

$$MSD(t) = \frac{1}{N}\sum_{i=1}^{N} < [r_i(t_0 + t) - r_i(t_0)]^2 >= B + 6D_c t \quad (2)$$

where N is the total number of atoms, $r_i(t_0 + t)$ and $r_i(t_0)$ are the positions at time $t_0 + t$ and t_0, respectively, B is a constant, and D is a self-diffusion coefficient.

Membrane preparation

After drying at 120 ˚C in a vacuum oven overnight, a measured quantity of POSS particles was dispersed in *n*-heptane solution under stirring at room temperature for 4 h. Then the PDMS polymer, TEOS (cross-linker), and dibutyltin dilaurate (catalyst) were added successively to the POSS/*n*-heptane suspension (*n*-heptane/PDMS/TEOS/dibutyltin dilaurate = 10:1:0.1:0.01, weight composition). The resulting POSS/PDMS casting solution was kept stirred for another 3-4 h. Subsequently, the casting solution was coated on the outer surface of the water-pretreated tubular ceramic support for 1 min through the dip-coating method. Following the removal of the solvent at room temperature for 24 h and then curing in the oven at 120 ˚C for another 12 h, the POSS/PDMS membrane was finally fabricated. The POSS content of these membranes was varied as 0, 10, 20, 30, and 40 wt.%, which means the POSS/PDMS membrane contained 0, 10, 20, 30, and 40 wt.% POSS nanoparticles, respectively.

Characterizations

Morphologies of POSS particles and POSS/PDMS membranes were examined by scanning electron microscope (Quanta-2000, FEI), atomic force microscope (DI-NS3a, Digital Instruments MultiMode), and transmission electron microscope (JEM-2010, UHR). For TEM characterization, membrane samples were fixed in epoxy and cut into slices by the technology of ultracryotomy (Leica EM UC7-FC7) at -160 °C with the speed of 1 mm/s. The ultrathin membrane samples with the thickness of 40-50 nm were then transferred to carbon-coated copper grids before observation. Thermal properties were determined with a differential scanning calorimeter (DSC, Q2000, TA Instruments), with nitrogen flow rate of 100 mL/min and temperature rate of 10 °C/min. IR spectra were recorded on a spectrophotometer (AVATAR-FT-IR-360, Thermo Nicolet) in the range of 4000-400 cm^{-1}. 32 scans were accumulated with a resolution of 4 cm^{-1} for each spectrum. The membrane crystal structures were obtained with an X-ray diffractometer (XRD, D8-advance, Bruker) using Cu Kα radiation, in the range of 5-40 ° with an increment of 0.05 ° at room temperature. Young's modulus of the membranes were obtained by using a dynamic mechanical analyzer (DMA, DMA-e7, Perkin-Elmer) under ambient conditions. Adsorption isotherms for n-butanol and water with POSS particles were obtained using an Intelligent Gravimetric Analyzer (IGA, IGA-100, Hiden analytical). The POSS particles were activated by heating to 100 °C and then tested at 40 °C by accurately controlling the pressure of vapour (water and *n*-butanol). The transient and equilibrium weight changes of the samples were measured and recorded for analysis. The static contact angles of membranes were measured by Sessile drop method using contact angles measurement system (DSA100, Kruss) at room temperature. The average contact angle was obtained by measuring the same sample at three different sites.

The pore radius of POSS and free volume sizes in the membranes were characterized by positron annihilation lifetime spectroscopy (PALS) in the R&D Center for Membrane Technology in Chung Yuan University in Taiwan[46-48]. A conventional fast-fast coincidence spectrometer with a time resolution of 250 ps was used. A radioactive source of 22Na (0.74 MBq), sealed in between 12-μm thick Kapton films, was sandwiched in two stacks of membrane samples that consisted of several layers of free-standing POSS/PDMS MMMs. Each stack of sample had a total thickness of 1 mm. Positron annihilation lifetimes were recorded using a fast-fast coincidence timing system. A time-to-amplitude converter was used to convert lifetimes and to store timing signals in a multi-channel analyzer (Ortec System). Two million counts were collected, and the lifetime distribution was determined using the PATFIT computer program[49] and Maximum Entropy for Lifetime Analysis (MELT) program[50] which is based on the Bayesian theorem and is implemented in MATLAB software. The mean free volume radius R can be related to *o*-Ps lifetime (τ_3) using a semi-empirical equation based on a spherical infinite potential well model[51]:

$$\tau_j = \frac{1}{2}\left[1 - \frac{R_j}{R_0} + \frac{1}{2\pi}\sin\left(\frac{2\pi R_j}{R_0}\right)\right]^{-1} \quad (3)$$

where τ_i (*o*-Ps lifetime, j=3 or 4) and R (free-volume hole radius) are expressed in ns and $\times 10^{-10}$ m (Å), respectively. R_0 is equal to $R + \Delta R$, where ΔR is a fitted empirical electron layer thickness = 1.66 Å determined by fitting well-known cavities.

Pervaporation test

The pervaporation experiment was conducted on a homemade apparatus, as described in our previous work[15]. The membrane was sealed in a stainless steel PV cell, with an effective membrane region of 15.80 cm^2. The feed solution was maintained at a preset temperature and circulated from the feed tank through the membrane cell at a flow rate of 15 L/h. During experiments, *n*-butanol was added to maintain a constant feed

concentration of 1 wt%. The vapor permeate was collected in a liquid nitrogen trap. The permeate pressure was below 400 Pa during the collections. *N*-butanol concentrations were determined with gas chromatography (GC-2014, SHIMADZU, Japan) equipped with a thermal conductivity detector (TCD) using a Porapak Q packed column and helium (He) as carrier gas. *I*-butanol was used as an internal standard. If the permeate separated into two phases, the permeate sample was diluted with deionized water to obtain a single phase prior to injection. To ensure reproducibility, all experimental results were repeated at least three times; the errors were less than 5 %.

The PV performance of a membrane is usually expressed in terms of the permeate flux and separation factor. Because the permeate flux is dependent on the operating conditions, normalizing the permeate flux with respect to the driving force will be useful to further understand the permeate-specific intrinsic membrane properties changed by the addition of POSS particles in the PDMS membrane. This intrinsic membrane properties are permeability P and selectivity α, which are defined based on the solution-diffusion mechanism[52].

$$P_i = \frac{J_i \times l}{P_{i,feed}^{vapor} - n_{i,permeate} \times p_{permeate}} \quad (4)$$

$$\alpha_{H_2O}^{BtOH} = \frac{P_{BtOH}}{P_{H_2O}} \quad (5)$$

where J_i is the partial permeate flux of component i, l is the membrane thickness, $P_{i,feed}^{vapor}$ is the equilibrium partial vapor pressure of i in the feed, $n_{i,permeate}$ is the mole fraction of i in the permeate, and $p_{permeate}$ is the permeate pressure; P_{BtOH} and P_{H_2O} are the permeability of *n*-butanol and water, respectively.

Results and discussion

Polymer chain conformation

Molecular diffusion in dense polymeric membrane is determined mainly by the polymer chain conformation. As for mixed matrix membranes, the incorporation of inorganic fillers would affect the packing and mobility of the polymer chain. Thus, the effect of incorporating POSS on the PDMS chain conformation was studied first by using both the MD simulation technique and experimental characterizations.

The packing of polymer chains could be studied by using RDF analyses in MD simulation, which entails intramolecular and intermolecular behavior of the polymer chains. The RDF spectra could indicate the probability density of atoms found at a specific distance. Generally, a higher peak intensity is related to the better ordering of atoms or larger molecular interactions in the molecular model[53]. In MD simulation process, PDMS chains were firstly selected from the POSS/PDMS MMMs cell, and then the Si and O atoms on the PDMS chains were selected in order to be distinguished from these atoms on POSS molecules. The calculated normalized RDF curves of Si and O atoms on PDMS chains are shown in Figure 3. Peaks that appeared at different positions are corresponded to different distances of Si and O atom locations in the PDMS structures. For each PDMS membrane, there are three sharp peaks in the short-distance region (0-5 Å) of the RDF curve (Figure 3a), which are attributed to the bonding distance of Si-O, Si-Si, and O-O atom pairs on PDMS chains, respectively. They reflect the intra-molecular packing and interaction in the PDMS membrane. Whereas the two broad peaks in the long-distance region (> 5 Å) are resulted from the non-bonding distance of Si and O atoms (Figure 3b), which suggest the inter-molecular packing and interaction of the polymer chains in PDMS membrane. It is found from the MD simulation that, with the increase in the POSS content of the PDMS MMMs, the RDF peak intensities increase gradually in the short-distance region, while they are kept almost constant in the long-distance region. The results indicate that the intra-molecular interaction of PDMS chains was promoted by the POSS incorporation, which made the packing of each PDMS chain more compact. It would lead to a smaller free volume size in the PDMS membrane. However, the inter-molecular packing and interaction of the PDMS chains were nearly not affected by the introduction of POSS. It may be attributed to the very flexible backbone of PDMS chain, as well as the good compatibility between methyl-POSS and PDMS.

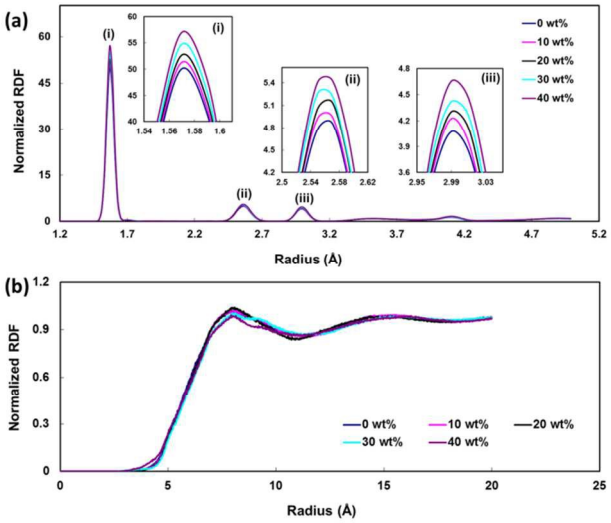

Fig. 3 RDF curves of Si and O atoms on PDMS chains from POSS/PDMS MMMs cells; POSS content: (a) 0 wt%, (b) 10 wt%, (c) 20 wt%, (d) 30 wt%, (e) 40 wt%

Furthermore, the MSD calculation of MD simulation could be adopted to investigate the mobility of polymers and inorganic fillers[54]. In this work, *MSD* and self-diffusion coefficients (D_c) of Si and O atoms in the PDMS chains and POSS molecules were calculated to study the molecular mobility of PDMS and POSS in the POSS/PDMS MMMs. In general, a larger slope or displacement in the MSD diagram indicates a higher molecular mobility. As shown in Figure 4a, incorporating POSS into the PDMS polymer leads to a significant advance in the mobility of PDMS backbone chains, which is further linearly improved by increasing the POSS content. E.g., D_c in PDMS MMMs filled with 40 wt% POSS is 0.267×10^{-10} m^2/s, which is ca. fourfold higher than that in the pristine PDMS membrane (0.071×10^{-10} m^2/s). The slopes were not very stable at the beginning and the end of the simulation process as the model was under unsteady states. Similar phenomena have been observed in literatures that related to the POSS/polymer composite system[42, 54-56]. Likewise, it is found in Figure 4b that the mobility of POSS molecules (i.e., relative motion of POSS molecules in the polymeric matrix) in the PDMS MMMs is also enhanced with the POSS content. A reasonable explanation for these phenomena is as follows: with the induction of inter-attractions of POSS molecules caused by electrostatic and van der Waals forces, the POSS molecules are prone to get closer that increases their mobility. Meanwhile, in the POSS/PDMS MMMs, the abundant molecular interactions

between POSS and PDMS would cause the adsorption of POSS molecules on the PDMS chains. The accelerating movement of POSS eventually improved the molecular mobility of PDMS. The advancement of chain mobility would create more cavities (free volumes) in the POSS-PDMS MMMs.

MD simulation demonstrated that the molecular interactions in the POSS/PDMS MMMs were the major driving force for the evolution of the PDMS chain conformation. Also, the packing and mobility behavior of the PDMS chains can be

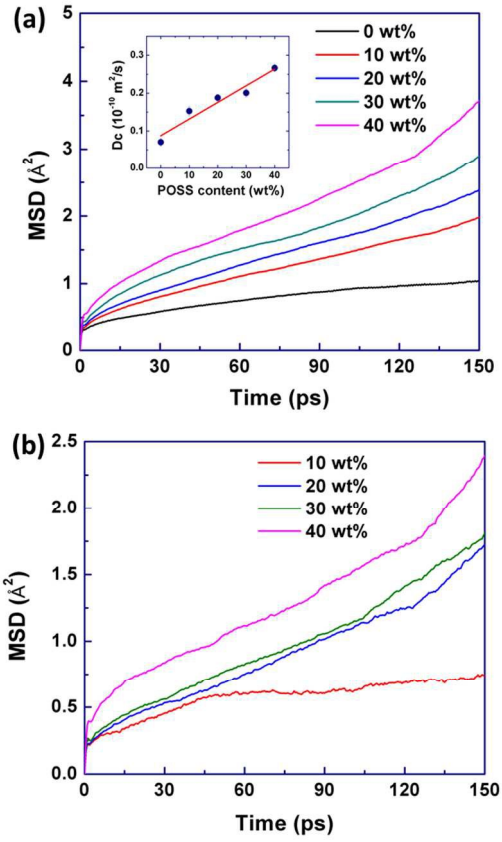

Fig. 4 MSD of Si and O atoms on (a) PDMS chains (inserted diagram gives the slopes of linear fitting of MSD *vs* time during 30-120 ps) and (b) POSS molecules

experimentally analyzed by DSC measurement[57]; the result is shown in Figure 5. By increasing the POSS content from 0 to 40 wt% in the MMMs, both the glass transition temperature (T_g) and the crystallinity (X_c) of the PDMS membrane are decreased linearly, from -116.5 ºC to -121.9 ºC and from 61.6% to 34.9%, respectively (Figure 5a); also the heat of cold crystallization (ΔH_c) and the heat of fusion (ΔH_f) show linear decline (Figure 5b). Ideally, the crystallinity of the PDMS membrane is related only to the PDMS content if the PDMS chains are not affected by external conditions (e.g., filler incorporation, polymer blending). In view of this, theoretical values of X_c in MMMs were calibrated based on the PDMS weight percent, and the result is given by the dash line in Figure 5a. Thus, the influences of incorporating POSS fillers on the crystallinity, cold crystallization, and melting behavior of the PDMS membrane can be reflected by the value difference between the solid line and the dash line. The result suggests that larger amounts of amorphous domains were produced in the PDMS membrane with the introduction of more POSS fillers, and thus the membrane crystallinity was reduced. The incorporation of POSS nano-particles could disrupt the crystallization process of PDMS polymer such that smaller crystallite sizes are achieved as well as changing the nucleation process from heterogeneous to homogeneous where the Avrami coefficient approaches one [58]. The resultant effect decreased the crystallization rate and extent of PDMS membrane, and thus there would be more spaces for the PDMS chain mobility. The above finding agrees well with RDF and MSD calculations from MD simulation results.

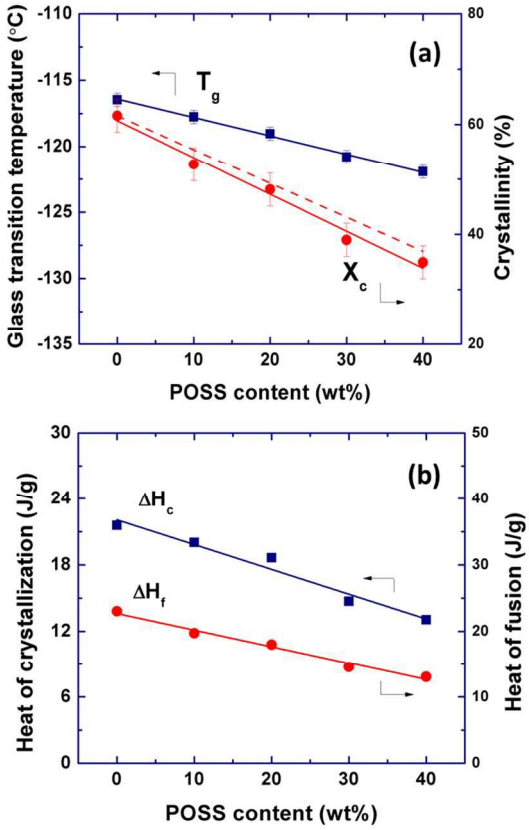

Fig. 5 Effects of POSS content on (a) *Tg* and *Xc* and (b) Δ*Hc* and Δ*Hf* of POSS/PDMS MMMs

Chemical and physical structures

Besides affecting the polymer chain conformation, the molecular interactions in MMMs would have more or less impact on the chemical and physical structures of the membrane. Figure 6a displays the ATR-FTIR spectra of POSS, PDMS, and MMMs. New adsorptions were not found in the POSS/PDMS MMM spectra; the peaks shown from POSS and PDMS[59, 60] are intrinsic. The result is in accordance with the physical incorporation of POSS to form MMMs, and chemical reaction could hardly happen between the methyl-POSS molecule and the hydroxyl-terminated PDMS chain. Nevertheless, the chemical groups of POSS show a coincident redshift ($\delta(CH_3)$: from 1270 to 1257 cm^{-1}; ν_{as}(Si-O-Si): from 1115 to 1082 cm^{-1}; ν(Si-C): from 776 to 767 cm^{-1}) in the POSS/PDMS MMMs. Similar results are also found in FTIR characterization (Figure S1 in ESI†). It could be attributed to two possibilities: the combination effect of the characteristic peaks of PDMS, and the presence of molecular interactions between Si-CH_3 and Si-O-Si groups on POSS and PDMS. Because both methyl-POSS and PDMS consist of Si-CH_3 and

Si-O-Si groups, it is difficult to confirm the primary cause just from the IR analysis.

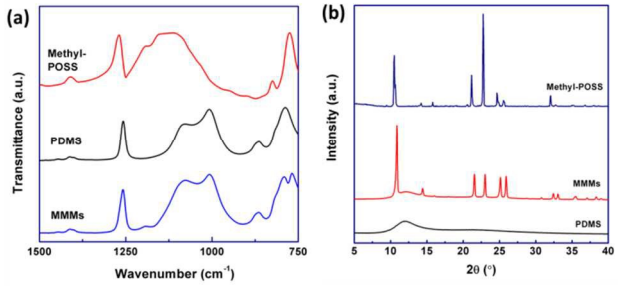

Fig. 6 (a) ATR-FTIR spectra and (b) XRD patterns of POSS particles, PDMS membrane, and POSS/PDMS MMMs

Furthermore, XRD was used to analyze the crystal structures of POSS, PDMS, and MMMs. As shown in Figure 6b, the characteristic peak at 12° of the cross-linked PDMS can also be found in the XRD pattern of MMMs. It indicates that the introduction of POSS fillers into the PDMS matrix has a little influence on the original d-spacing (7.38 Å) of the PDMS tetragonal crystal lattice. This result is well in line with the RDF analysis of MD simulation, in which the inter-molecular interaction and packing density in the non-bonding region (> 5 Å) almost did not change with the POSS incorporation. But the crystalline POSS was slightly affected by the PDMS matrix, resulting in a 0.1-0.2° right shifting of the characteristic peaks and variations in the peak intensity of the POSS crystals in the XRD pattern of MMMs.

In addition, the Young's modulus of the membranes was determined using DMA, and the results are shown in Figure S2 in ESI.† Because of good mechanical strength of POSS particles[61], as well as the formed interfacial interactions between POSS and PDMS, the tensile deformation of PDMS chains was effectively suppressed by incorporating POSS into the PDMS matrix. Thus, Young's Modulus of the membrane is greatly increased with the POSS loading. The improvement in mechanical strength is conducive to the installation of the membrane module and the long-term stability of MMMs.

Morphology

As reported by a number of literatures, favorable molecular interactions could be beneficial for the dispersion of POSS in PDMS and the interfacial morphology of POSS-PDMS. Figure 7a shows the casting solution and a dense POSS/PDMS MMM. It can be clearly observed that POSS particles are uniformly dispersed in the PDMS solution, and the resulting dense MMM also displays a homogeneous appearance. To improve the membrane flux for practical applications, the POSS/PDMS solution was coated on the surface of tubular porous ceramic substrates to form ceramic-supported composite polymeric membranes with a thin active layer for separation, as reported in our previous work[62, 63]. A typical cross-sectional SEM image of the as-prepared ceramic-supported POSS/PDMS MMM is given in Figure 7b. The POSS/PDMS separation layer, firmly deposited on the ceramic substrate, is homogeneous and defect-free, with a thickness of ca. 9 μm. From the enlarged cross-sectional SEM image (Figure S3a in ESI†), it is more clear to find that the POSS particles are uniformly dispersed in PDMS matrix. The fine structure of the interfacial morphology of POSS/PDMS was observed with TEM, as displayed in Figure 7c-d. Although both POSS and PDMS consist of Si-O-Si and -CH_3 groups, differences in molecular structures and crystallinity cause light and shade variations under the TEM characterization. The dark area is related to the POSS dispersed phase, and the light area corresponds to the PDMS continuous phase. As seen in Figure 7c, the POSS particles are found to be tightly embedded in the PDMS domain without interfacial voids. This widespread morphology is further confirmed by a lower magnification of TEM image of Figure S3b in ESI.† Meanwhile, the enlarged image in Figure 7d distinctly reveals good compatibility between POSS and PDMS phases. PDMS chains are well adsorbed on the POSS surface, with an interfacial thickness of ca. 1-2 nm, corresponding to the length of 6-12 PDMS repeat units. By integrating the results of MD simulation, it can be reasonably inferred that this well-defined filler-polymer interfacial morphology could play two roles in determining the microstructures of MMMs: one is improving the intra-molecular interaction of segmental PDMS chains in the interface, while maintaining the flexibility of the main PDMS chains; the other is utilizing the interactions (i.e., electrostatic and van der Waals forces) between POSS molecules that adsorbed on the PDMS chain to promote the molecular mobility of the PDMS chains.

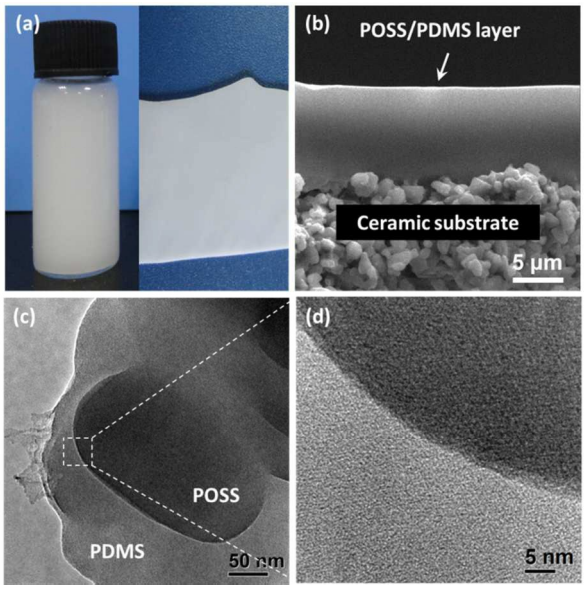

Fig. 7 (a) Digital photos of dip-coating solution and symmetric POSS/PDMS MMM; (b) cross-sectional SEM image of ceramic-supported composite POSS/PDMS membrane; (c-d) TEM images of POSS/PDMS MMM. (POSS content: 40 wt%)

The MMMs surface morphologies were characterized by SEM and AFM, and the results are given in Figure 8. As shown in Figure 8a, in contrast to the smooth surface of the pristine PDMS membrane, uniform concave-convex surfaces of the POSS/PDMS MMMs are found, and the area and numbers of these sunken and bulges are increased with the POSS content. The phenomena could be seen more clearly in the 2D and 3D surface AFM images in Figure 8b-c. By incorporating POSS fillers, the even PDMS membrane surface become wrinkled, the degree of which is magnified with the rise of the POSS loading in the MMMs. As a consequence, the membrane roughness increases linearly, the R_q (mean square roughness) is enlarged from 17.4 nm to 571 nm for the MMMs filled with 40 wt% POSS. Compared with the morphology of POSS particles (Figure S4 in ESI†), it can be inferred that no POSS particles are found in the SEM surface images (Figure 8a). Moreover,

according to the AFM phase images (Figure 8d), only PDMS phase was observed in the membrane surface. Thus, we speculate that the generation of the concave-convex and plicated surface in the MMMs results mainly from the variation in internal stress during the solvent volatilization of the membrane fabrication. The stress variation is probably due to the enhancement of the PDMS chain mobility, induced by the molecular interactions of POSS adsorbed on the PDMS chain.

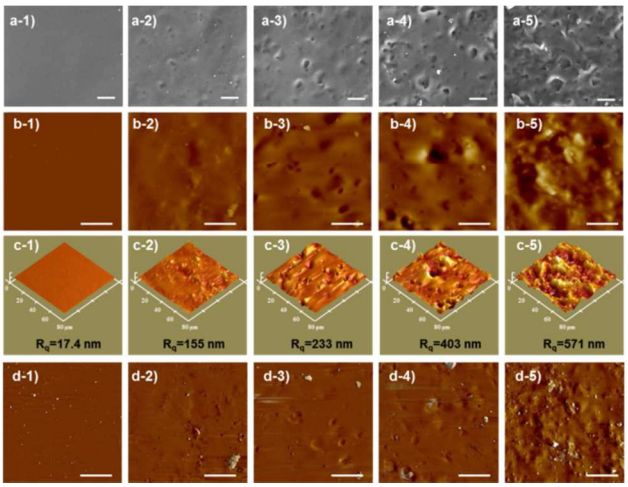

Fig. 8 (a) Surface SEM images; (b) 2D surface AFM images; (c) 3D surface AFM images; (d) AFM phase images of POSS/PDMS MMMs (bar in all images: 20 μm; -1) to -5) correspond to POSS content of 0, 10, 20, 30, 40 wt% in MMMs)

Free volume distribution

The above-mentioned evolution of polymer chain conformation and microstructure induced by molecular interactions would also have a significant influence on the free volume elements (i.e., cavities or holes) of MMMs. Molecular diffusion in dense polymeric membranes is strongly dependent on free volumes in polymer, which provide diffusion channels with low transport resistance. Free volumes are created by inefficient chain packing and transient gaps generated by thermally induced chain mobility[64]. Lee and co-workers demonstrated that free volume topologies of glass polymers could be systematically tailored by thermally driven segment rearrangement[5]. Our previous work also found that centrifugal force is effective to optimize the free volumes by arrangement and orientation of molecular chains in polyamide membranes[65].

In recent years, positron annihilation spectroscopy (PAS) technique has been proven as an advanced and powerful tool in analyzing the free volume size and distribution for various polymers for molecular separations[5, 38, 48]. PAS results of POSS/PDMS MMMs are shown in Figure S3 (ESI†), Table S1(ESI†) and Figures 9-10. The positron lifetimes τ_3 and τ_4 are due to *o*-Ps annihilation. In polymeric materials, the annihilation lifetime is on the order of 1-5 ns, which results from the so-called pickoff annihilation with electrons in molecules. According to Equation 3, the positron lifetime can be used to calculate the mean free volume radius R. Table S1 shows that the positron annihilation time in the PDMS membrane exhibits a bimodal distribution (τ_3 = 1.241 ns and τ_4 = 3.135 ns), corresponding to a free volume size distribution at two ranges, with an average small radius of R_3 = 0.202 nm and large radius of R_4 = 0.373 nm. Similar results for PDMS membranes in the literature[66, 67] were found. A POSS molecule with a flexible cage structure also owns diffusion channels for molecular transport; its free volume radius R_4 is 0.362 nm. It is noted that the *o*-Ps annihilation intensity I_4 of POSS (4.99%) is much lower than that of PDMS, which is probably due to that PALS data is strongly dependent on the physicochemical property of the material[35]. Although they have similar chemical elements and groups (e.g., Si-O-Si, -CH_3), their structures are much different. POSS owns a cage-like structure made by single Si-O-Si unit, while PDMS possesses a cross-linked network consisted of several Si-O repeat units. It would lead to the different free volume elements, namely lifetime and intensity of positron annihilation. Most positron annihilation in POSS may be attributed to short lifetimes (τ_1, τ_2).

We found in the PAS analysis of POSS/PDMS MMMs that the addition of POSS to PDMS brought regular variations in the membrane free volumes. As presented in Table 1 and Figure 10, with an advance of the POSS loading, the small free volume elements decline progressively, with R_3 moving to smaller size, while the large volume elements gradually increase, with R_4 moving to larger size. Meanwhile, the small

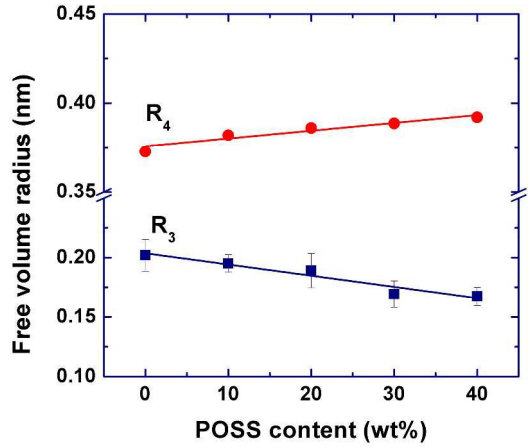

Fig. 9 Effect of POSS content on free volume sizes of POSS/PDMS MMMs

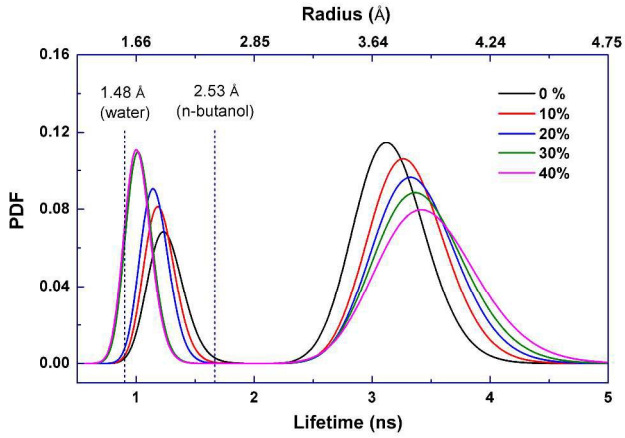

Fig. 10 Free volume distribution for POSS/PDMS MMMs

free volume intensity I_3 increases and the large free volume intensity I_4 decreases, maybe owing to the partial pore blockage of POSS by PDMS chains[30]. As shown in Figure 9, there are linear relations both for R_3 and R_4 changes with the POSS content in the MMMs. As for the MMMs with 40 wt% POSS, R_3 is reduced to 0.167 nm and R_4 increased to 0.392 nm. Although the intrinsic free volume radius of POSS is smaller

than that of the pristine PDMS membrane, R_4 for the PDMS membrane was greatly enlarged after the incorporation of POSS (i.e., R_4 increases from 0.373 nm to 0.392 nm). The result suggests that free volumes in MMMs could be finely tuned by molecular interactions with two possible aspects: (i) increase in the PDMS intramolecular packing reduces the small free volumes (R_3), and (ii) improvement in the PDMS chain mobility enhances the large free volumes (R_4).

It is demonstrated that our proposed simple physical incorporation of nano-sized POSS could realize the true molecular-scale regulation of the polymer chain packing and mobility, because the variation in the free volume radius is just ca. 0.02-0.035 nm. For the molecular-level separation occurrence in dense polymeric membranes, only less than 0.02 nm difference in the penetrant size is enough to yield substantial differences in the flux through polymeric membranes. For instance, although the difference in the molecular kinetic diameters of O_2 and N_2 is only 0.018 nm, the permeance ratio of O_2 and N_2 (selectivity) could be as high as 8 in strongly size-sieving polymeric membranes[68].

The above special characteristics of tunable free volumes in POSS/PDMS MMMs are profitable for selective-permeating larger-sized molecules. It is because the shrunken small free volumes hinder the smaller-sized molecule diffusion, while the extended large free volumes facilitate the larger-sized molecule diffusion. The effect of the polymer free volume on the molecular diffusion coefficient is usually modeled by the statistical mechanics description of diffusion in a liquid of hard spheres, proposed by Cohen and Turnbull[69] as follows:

$$\boldsymbol{D = A\exp(\frac{-\gamma V^*}{V_f})} \quad (6)$$

where A is a pre-exponential factor that is weakly dependent on temperature, γ an overlap factor introduced to avoid double-counting of free volume elements, V^* the minimum free volume size that can accommodate a penetrant molecule (and is closely related to the penetrant size), V_f the average free volume in the polymer accessible to penetrants for transport. Based on the Solution-diffusion model, the diffusion selectivity $\alpha_{D_{i/j}}$ can be expressed as below:

$$\boldsymbol{\alpha_{D_{i/j}} = \frac{D_i}{D_j} = \exp(\frac{\gamma_j V_j^* - \gamma_i V_i^*}{V_f})} \quad (7)$$

where i and j represents penetrant i and j, respectively.

According to Equation 6, with the increase in free volumes in polymeric membranes, the diffusion coefficient of penetrant increases and then the membrane permeability is enhanced. Based on Equation 7, if the molecular size of penetrant j is larger than that of penetrant i, generally $\gamma_j V_j^* > \gamma_i V_i^*$, resulting in $\alpha_{D_{i/j}} > 1$, namely smaller-sized molecules are preferentially diffused in the membrane. However, $\alpha_{D_{i/j}}$ declines with the enlargement of V_f and finally approaches 1. That is to say, enlarging the membrane free volumes would be in favor of weakening the diffusion selectivity for smaller-sized molecules (i.e., size-sieving ability) to facilitate the selective diffusion of larger-sized molecules. For instance, the recovery of butanol from aqueous solution through polymeric membranes is a typical application of the selective permeation of larger-sized molecules (butanol) over smaller-sized molecules (water).

Sorption property

Besides of the diffusion process, the separation performance is also dependent on the sorption process according to the solution-diffusion theory[52]. Therefore, the surface sorption property of the POSS/PDMS MMMs was evaluated by contact angle test, using water and butanol as the contacting liquid, respectively. Because of the intrinsic hydrophobicity and organophilicity, the PDMS MMMs general show water contact angle > 90 º and butanol contact angle < 90 º, as displayed in Figure 11a. Thus, most PDMS-based membranes exhibited high sorption selectivity for butanol over water in literature[13, 14, 40, 70]. With incorporating POSS particles, the water contact angles are decreased a lot while the butanol contact angles have some fluctuation. The result suggests that the hydrophobicity of the POSS/PDMS MMMs was lower than that of the pristine PDMS membrane.

To further verify the role of POSS played in the sorption process, the adsorption isotherm of *n*-butanol and water on POSS particles were respectively measured by varying the vapor pressure from 0 to 26 kPa at 40 ºC. As shown in Figure 11b, the uptake of water is higher than that of butanol, indicating a water-selective sorption property of POSS filler. Moreover, the adsorbed amounts of both water and butanol are much lower than that of the porous materials such as silicalite-1 zeolite[28], ZIF-8 MOFs[16]. It means that these molecules could hardly enter into the POSS cage and POSS fillers in the PDMS MMMs would have little contribution to the sorption process when separating alcohol/water mixtures.

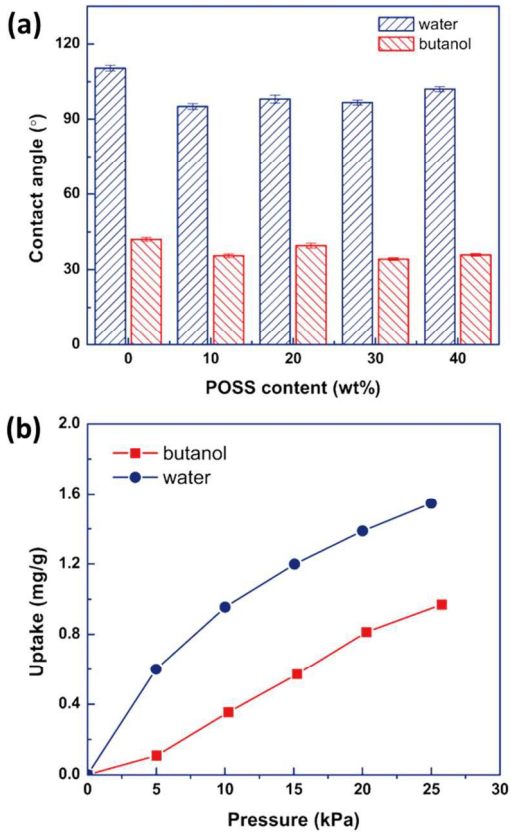

Fig. 11 (a) Contact angles of water and *n*-butanol on POSS/PDMS MMMs surfaces; (b) Adsorption isotherms of water and *n*-butanol on POSS particles at 40 ºC.

Separation performance

The as-prepared POSS/PDMS MMMs were applied to pervaporation recovery of *n*-butanol from a 1 wt% aqueous solution at 40 ºC. As shown in Figure 12, the separation performance of the PDMS membrane is greatly improved by

the POSS incorporation: both the butanol permeability and selectivity increase simultaneously with the POSS content. Especially for the PDMS MMMs with 40 wt% POSS,

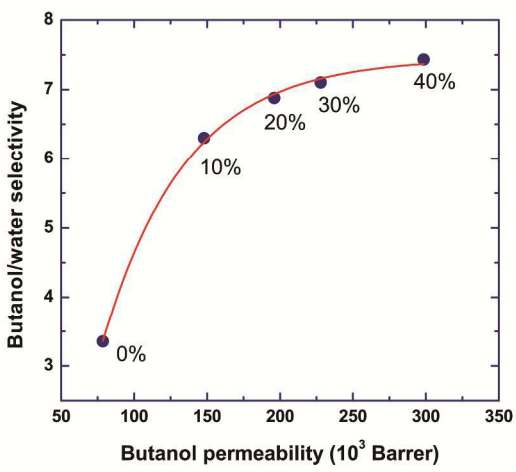

Fig. 12 Butanol permeability and selectivity of POSS/PDMS MMMs (Feed: 1 wt% n-butanol/water solution at 40 ºC)

the permeability and selectivity are respectively 3.8- and 2.2-times higher compared with the pristine PDMS membrane. From the SEM and TEM characterizations in Figure 7, there are no visible interfacial defects in our POSS/PDMS MMMs. Thus it is reasonable to speculate that the rational construction of molecular interactions between POSS and PDMS could highly reduce the interfacial defects, which are generally observed in conventional zeolite/polymer MMMs. More importantly, the free volumes in the PDMS membrane could be finely regulated for the fast selective permeation of larger-sized molecules.

The kinetic diameters of *n*-butanol (0.505 nm) and water (0.296 nm) are just located in the ranges of small free volume diameters ($2 \times R_3$ = 0.334-0.404 nm) and large free volume diameters ($2 \times R_4$ = 0.746-0.784 nm), respectively, of the POSS/PDMS membranes. Their relationships are marked in Figure 11. The schematic of the effects of the POSS incorporation on the membrane free volume variations and the separation of butanol/water is displayed in Figure 13.

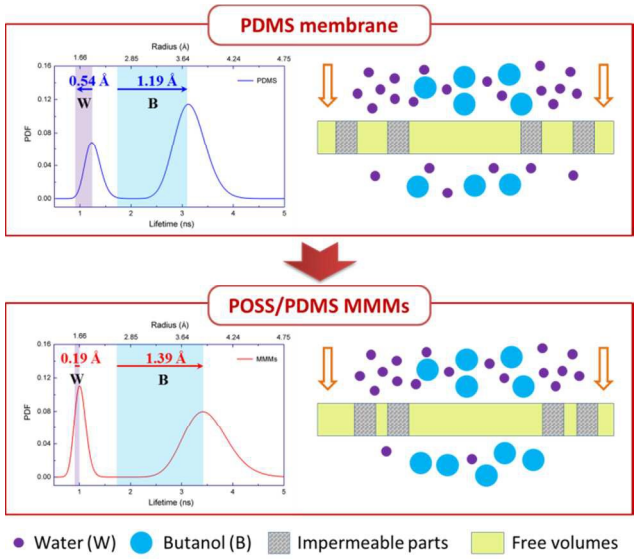

Fig. 13 Schematic of tuning membrane free volumes and its effect on separation process

In the POSS/PDMS MMMs, the decrease in small free volume (R_3) can effectively hinder the water diffusion, and the increase in large free volume (R_4) is good for promoting the butanol diffusion. According to Equation 9, the R_4 enlargement is also beneficial for improving the diffusion selectivity for butanol. Although there is a possibility of butanol molecules diffusing through the small free volume (R_3) as it gets swollen by the feed, the large free volumes are considered as the main diffusion pathways for butanol molecules. Therefore, POSS/PDMS MMMs could exhibit both high butanol permeability and selectivity, breaking the existing trade-off between permeability and selectivity in polymeric membranes.

The reported separation performance of organophilic membranes for the butanol recovery from aqueous solutions is displayed in Figure 14 and Table S1 (ESI†). To eliminate the effect of operating conditions (feed temperature and composition) on the separation performance, the membrane flux and separation factor were normalized to permeance and selectivity, respectively. Then, intrinsic membrane properties could be fairly compared[71]. Because some of the reported membrane thicknesses are unknown, permeance was used for comparison (1 GPU = 1×10^{-6} cm^3 (STP) $cm^{-2}s^{-1}cmHg^{-1}$). It can be found that the POSS/PDMS MMM exhibits the highest butanol/water selectivity, as well as a very high butanol permeance. The performance of the POSS/PDMS membrane clearly transcends the upper bound of the state-of-the-art organophilic pervaporation membranes.

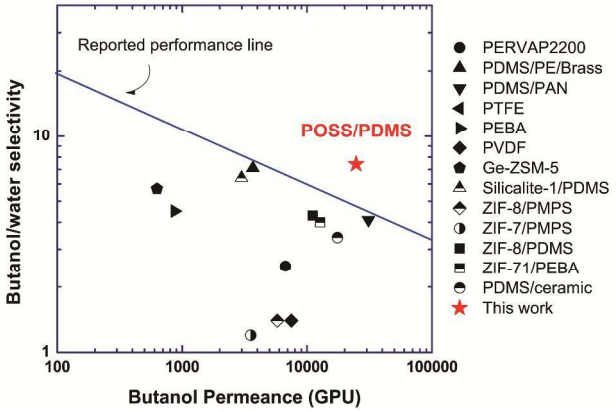

Fig. 14 PV performance of organophilic membranes in butanol/water solution (Membranes reported in literature: PERVAP2200[12], PDMS/PE/Brass[13], PDMS/PAN[14], PTFE[22], PEBA[19], PVDF[21], Ge-ZSM-5[23], Silicalite-1/PDMS[18], ZIF-8/PMPS[16], ZIF-7/PMPS[16], ZIF-8/PDMS[17], ZIF-71/PEBA[20], PDMS/ceramic[15].)

Conclusions

In summary, we have designed and fabricated high-performance POSS/PDMS MMMs with tunable free volumes driven by favorable filler-polymer molecular interactions. Molecular dynamics simulation indicated that the POSS incorporation enhanced the PDMS chain intra-molecular interactions and, at the same time, improved the PDMS chain mobility. Thus, in the PDMS MMMs, small free volumes were reduced and large free volumes increased. The feature of tunable free volumes was beneficial for the preferential permeation of large-sized molecules through the polymeric membrane. In the bio-butanol recovery from aqueous solutions,

the obtained POSS/PDMS MMMs improved both the permeability and the selectivity of the pristine PDMS membrane by 3.8- and 2.2- times, respectively, which overcame the permeability-selectivity trade-off limitation of polymeric membranes. Moreover, the separation performance of the MMMs clearly transcended the upper bound of the state-of-the-art organophilic pervaporation membranes. The above characteristics of the POSS/PDMS MMMs obtained through molecular-interaction-driven tuning of free volumes make them to be a great promising candidate for practical applications in the bio-fuel production. Also, the proposed approach based on rationally creating molecular interactions can be expected to have broad applicability in fabricating high-quality MMMs for molecular separations.

Acknowledgements

This work was supported by the Innovative Research Team Program by the Ministry of Education of China (No. IRT13070), National Natural Science Foundation of China (Nos. 21406107, 21476107) and Natural Science Foundation of Jiangsu Province (No. BK20140930).

Notes and references

[a] State Key Laboratory of Materials-Oriented Chemical Engineering, College of Chemistry and Chemical Engineering, Nanjing Tech University (former Nanjing University of Technology), 5 Xinmofan Road, Nanjing 210009, PR China.
E-mail: wqjin@njtech.edu.cn (Prof. W.Q. Jin); Tel.: +86 25 83172266
[b] R&D Center for Membrane Technology, Department of Chemical Engineering, Chung Yuan University, Chung-Li 32023, Taiwan.
E-mail: krlee@cycu.edu.tw (Prof. K.R. Lee); Tel.: +886 3 2654190
† Electronic Supplementary Information (ESI) available: DMA analysis of membranes, SEM images of POSS particles and performance comparison of organophilic membranes for *n*-butanol recovery from aqueous solution. See DOI: 10.1039/b000000x/

1. M. A. Hickner, H. Ghassemi, Y. S. Kim, B. R. Einsla and J. E. McGrath, *Chemical Reviews*, 2004, 104, 4587-4612.
2. J.-T. Chen, Y.-J. Fu, Q.-F. An, S.-C. Lo, S.-H. Huang, W.-S. Hung, C.-C. Hu, K.-R. Lee and J.-Y. Lai, *Nanoscale*, 2013, 5, 9081-9088.
3. X. Zhang, D. Liu, D. Xu, S. Asahina, K. A. Cychosz, K. V. Agrawal, Y. Al Wahedi, A. Bhan, S. Al Hashimi, O. Terasaki, M. Thommes and M. Tsapatsis, *Science*, 2012, 336, 1684-1687.
4. J. Abramson and A. S. Vartanian, *Science*, 2013, 340, 1294-1295.
5. H. B. Park, C. H. Jung, Y. M. Lee, A. J. Hill, S. J. Pas, S. T. Mudie, E. Van Wagner, B. D. Freeman and D. J. Cookson, *Science*, 2007, 318, 254-258.
6. H. Q. Lin, E. Van Wagner, B. D. Freeman, L. G. Toy and R. P. Gupta, *Science*, 2006, 311, 639-642.
7. Z. Lai, G. Bonilla, I. Diaz, J. G. Nery, K. Sujaoti, M. A. Amat, E. Kokkoli, O. Terasaki, R. W. Thompson, M. Tsapatsis and D. G. Vlachos, *Science*, 2003, 300, 456-460.
8. Y. Li and T.-S. Chung, *International Journal of Hydrogen Energy*, 2010, 35, 10560-10568.
9. R. K. Joshi, P. Carbone, F. C. Wang, V. G. Kravets, Y. Su, I. V. Grigorieva, H. A. Wu, A. K. Geim and R. R. Nair, *Science*, 2014, 343, 752-754.
10. N. Qureshi and T. C. Ezeji, *Biofuels, Bioproducts and Biorefining*, 2008, 2, 319-330.
11. N. Qureshi and H. P. Blaschek, *Biomass and Bioenergy*, 1999, 17, 175-184.
12. E. El-Zanati, E. Abdel-Hakim, O. El-Ardi and M. Fahmy, *Journal of Membrane Science*, 2006, 280, 278-283.
13. S.-Y. Li, R. Srivastava and R. S. Parnas, *Journal of Membrane Science*, 2010, 363, 287-294.
14. J. Niemistö, W. Kujawski and R. L. Keiski, *Journal of Membrane Science*, 2013, 434, 55-64.
15. G. P. Liu, F. J. Xiangli, W. Wei, S. N. Liu and W. Q. Jin, *Chemical Engineering Journal*, 2011, 174, 495-503.
16. X. L. Liu, Y. S. Li, G. Q. Zhu, Y. J. Ban, L. Y. Xu and W. S. Yang, *Angewandte Chemie-International Edition*, 2011, 50, 10636-10639.
17. H. Fan, Q. Shi, H. Yan, S. Ji, J. Dong and G. Zhang, *Angewandte Chemie International Edition*, 2014, 53, 5578-5582.
18. J. Huang and M. M. Meagher, *Journal of Membrane Science*, 2001, 192, 231-242.
19. F. Liu, L. Liu and X. Feng, *Separation and Purification Technology*, 2005, 42, 273-282.
20. S. Liu, G. Liu, X. Zhao and W. Jin, *Journal of Membrane Science*, 2013, 446, 181-188.
21. K. Srinivasan, K. Palanivelu and A. Navaneetha Gopalakrishnan, *Chemical Engineering Science*, 2007, 62, 2905-2914.
22. D. L. Vrana, M. M. Meagher, R. W. Hutkins and B. Duffield, *Separation Science and Technology*, 1993, 28, 2167-2178.
23. S. Li, V. A. Tuan, J. L. Falconer and R. D. Noble, *Microporous and Mesoporous Materials*, 2003, 58, 137-154.
24. C. M. Zimmerman, A. Singh and W. J. Koros, *Journal of Membrane Science*, 1997, 137, 145-154.
25. T. S. Chung, L. Y. Jiang, Y. Li and S. Kulprathipanja, *Progress in Polymer Science*, 2007, 32, 483-507.
26. D. L. Gin and R. D. Noble, *Science*, 2011, 332, 674-676.
27. T. H. Bae, J. S. Lee, W. L. Qiu, W. J. Koros, C. W. Jones and S. Nair, *Angewandte Chemie-International Edition*, 2010, 49, 9863-9866.
28. N. L. Le, Y. Wang and T.-S. Chung, *Journal of Membrane Science*, 2011, 379, 174-183.
29. N. L. Le and T.-S. Chung, *Journal of Membrane Science*, 2014, 454, 62-73.
30. N. L. Le, Y. P. Tang and T.-S. Chung, *Journal of Membrane Science*, 2013, 447, 163-176.
31. Q. G. Zhang, B. C. Fan, Q. L. Liu, A. M. Zhu and F. F. Shi, *Journal of Membrane Science*, 2011, 366, 335-341.
32. R. Konietzny, T. Koschine, K. Rätzke and C. Staudt, *Separation and Purification Technology*, 2014, 123, 175-182.
33. D. B. Cordes, P. D. Lickiss and F. Rataboul, *Chemical Reviews*, 2010, 110, 2081-2173.
34. M. L. Chua, L. Shao, B. T. Low, Y. Xiao and T.-S. Chung, *Journal of Membrane Science*, 2011, 385–386, 40-48.
35. F.-J. Fu, S. Zhang, S.-P. Sun, K.-Y. Wang and T.-S. Chung, *Journal of Membrane Science*, 2013, 443, 144-155.
36. S. C. Chen, X. Z. Fu and T.-S. Chung, *Desalination*, 2014, 335, 17-26.
37. T. T. Moore and W. J. Koros, *Journal of Molecular Structure*, 2005, 739, 87-98.
38. T. C. Merkel, B. D. Freeman, R. J. Spontak, Z. He, I. Pinnau, P. Meakin and A. J. Hill, *Science*, 2002, 296, 519-522.
39. S. Roy, B. J. Lee, Z. M. Kakish and S. C. Jana, *Macromolecules*, 2012, 45, 2420-2433.
40. G. P. Liu, W. Wei and W. Q. Jin, *ACS Sustainable Chemistry & Engineering*, 2014, 2, 546-560.
41. B. Li, F. Pan, Z. Fang, L. Liu and Z. Jiang, *Industrial & Engineering Chemistry Research*, 2008, 47, 4440-4447.
42. K.-S. Chang, Y.-C. Chung, T.-H. Yang, S. J. Lue, K.-L. Tung and Y.-F. Lin, *Journal of Membrane Science*, 2012, 417–418, 119-130.
43. S. Nose, *Molecular Physics*, 1984, 52, 255-268.
44. H. J. C. Berendsen, J. P. M. Postma, W. F. van Gunsteren, A. DiNola and J. R. Haak, *The Journal of Chemical Physics*, 1984, 81, 3684-3690.
45. H. Sun, *The Journal of Physical Chemistry B*, 1998, 102, 7338-7364.
46. H. Chen, W.-S. Hung, C.-H. Lo, S.-H. Huang, M.-L. Cheng, G. Liu, K.-R. Lee, J.-Y. Lai, Y.-M. Sun, C.-C. Hu, R. Suzuki, T. Ohdaira, N. Oshima and Y. C. Jean, *Macromolecules*, 2007, 40, 7542-7557.
47. S.-H. Huang, W.-S. Hung, D.-J. Liaw, C.-L. Li, S.-T. Kao, D.-M. Wang, M. D. Guzman, C.-C. Hu, Y. C. Jean, K.-R. Lee and J.-Y. Lai, *Macromolecules*, 2008, 41, 6438-6443.
48. W.-S. Hung, M. De Guzman, S.-H. Huang, K.-R. Lee, Y. C. Jean and J.-Y. Lai, *Macromolecules*, 2010, 43, 6127-6134.
49. P. Kirkegaard, M. Eldrup, O. E. Mogensen and N. J. Pedersen, *Computer Physics Communications*, 1981, 23, 307-335.
50. A. Shukla, M. Peter and L. Hoffmann, *Nuclear Instruments and Methods in Physics Research Section A: Accelerators, Spectrometers, Detectors and Associated Equipment*, 1993, 335, 310-317.
51. S. J. Tao, *The Journal of Chemical Physics*, 1972, 56, 5499-5510.

52. J. G. Wijmans and R. W. Baker, *Journal of Membrane Science*, 1995, 107, 1-21.
53. K. Choi and W. H. Jo, *Macromolecules*, 1995, 28, 8598-8603.
54. Q. G. Zhang, Q. L. Liu, S. P. Huang, W. W. Hu and A. M. Zhu, *Journal of Materials Chemistry*, 2012, 22, 10860-10866.
55. Q. G. Zhang, Q. L. Liu, J. Y. Wu, Y. Chen and A. M. Zhu, *Journal of Membrane Science*, 2009, 342, 105-112.
56. Y. Yani and M. H. Lamm, *Polymer*, 2009, 50, 1324-1332.
57. J. Zhong, G. Lin, Wen, A. A. Jones, S. Kelman and B. D. Freeman, *Macromolecules*, 2005, 38, 3754-3764.
58. M. Avrami, *The Journal of Chemical Physics*, 1940, 8, 212-224.
59. B. Handke, W. Jastrzębski, W. Mozgawa and A. Kowalewska, *Journal of Molecular Structure*, 2008, 887, 159-164.
60. D. Cai, A. Neyer, R. Kuckuk and H. M. Heise, *Journal of Molecular Structure*, 2010, 976, 274-281.
61. Y. Liu, Z. Shi, H. Xu, J. Fang, X. Ma and J. Yin, *Macromolecules*, 2010, 43, 6731-6738.
62. F. J. Xiangli, Y. W. Chen, W. Q. Jin and N. P. Xu, *Industrial & Engineering Chemistry Research*, 2007, 46, 2224-2230.
63. W. Wei, S. S. Xia, G. P. Liu, X. L. Dong, W. Q. Jin and N. P. Xu, *Journal of Membrane Science*, 2011, 375, 334-344.
64. G. Choudalakis and A. D. Gotsis, *Current Opinion in Colloid & Interface Science*, 2012, 17, 132-140.
65. Q. F. An, W. S. Hung, S. C. Lo, Y. H. Li, M. De Guzman, C. C. Hu, K. R. Lee, Y. C. Jean and J. Y. Lai, *Macromolecules*, 2012, 45, 3428-3435.
66. S. J. Lue, C. L. Tsai, D.-T. Lee, K. P. O. Mahesh, M. Y. Hua, C.-C. Hu, Y. C. Jean, K.-R. Lee and J.-Y. Lai, *Journal of Membrane Science*, 2010, 349, 321-332.
67. M. F. F. Marques, P. M. Gordo, Z. Kajcsos, C. L. Gil, A. P. de Lima, D. P. Queiroz and M. N. de Pinho, *Radiation Physics and Chemistry*, 2007, 76, 129-133.
68. L. M. Robeson, *Journal of Membrane Science*, 2008, 320, 390-400.
69. M. H. Cohen and D. Turnbull, *Journal of Chemical Physics*, 1959, 31, 1164-1169.
70. G. P. Liu, W. Wei, H. Wu, X. L. Dong, M. Jiang and W. Q. Jin, *Journal of Membrane Science*, 2011, 373, 121-129.
71. R. W. Baker, J. G. Wijmans and Y. Huang, *Journal of Membrane Science*, 2010, 348, 346-352.

Graphic Abstract

Favorable molecular interactions were constructed to control polymer chain conformation to fabricate mixed matrix membranes with tunable free volumes, exhibiting simultaneously improved butanol permeability and selectivity.